INFLUENCE OF HYDROSTATIC PRESSURE ON DYNAMIC DIELECTRIC CHARACTERISTICS OF RbHSO$_4$

A. S. Vdovych[1] , R. R. Levitskii[1], I. R. Zachek[2], A. P. Moina[1]
[1]*Institute for Condensed Matter Physics of the National Academy of Sciences of Ukraine,*
1, Svientsitskii St., Lviv, UA-79011, Ukraine,
[2]*National University "Lviv Polytechnic",*
12, Bandery St., Lviv, UA-79013, Ukraine

Within the modified four-sublattice pseudospin model of deformed RbHSO$_4$ ferroelectrics, using the Glauber method and the mean field approximation, we calculate the dynamic dielectric permittivity of a mechanically clamped crystal and explore its dependence on hydrostatic pressure in wide temperature and frequency ranges. A satisfactory quantitative agreement with the experimental data is obtained.

Key words: ferroelectrics, dielectric permittivity, pressure effects.

I. INTRODUCTION

The RbHSO$_4$ crystal is an interesting subject of study, because it is sensitive to the influence of hydrostatic and uniaxial pressure or electric field (see [1]). At $T = 263.65$ K [2] it undergoes the phase transition from the high-temperature paraelectric phase to the low-temperature ferroelectric phase; the spontaneous polarization is directed along the c-axis (Fig. 1,a). The crystal is monoclinic (the space group $P2_1/c$ in the paraelectric phase and P/c in the ferroelectric phase) [3–5].

The phase transition is associated with the order-

ing of the sulphate groups $(SO_4)_{1f}$ in one of the two asymmetric positions.

In order to describe the dielectric, piezoelectric, and elastic characteristics of RbHSO$_4$ in [1, 6–9], the four-sublattice pseudospin model of RbHSO$_4$ with asymmetric double-well potential has been proposed, which also takes into account the piezoelectric coupling of the pseudospin and lattice subsystems. This model allowed us to obtain a qualitatively correct description of experimental data for the elastic constants and a quantitively correct description of the dielectric and thermal properties of this crystal, as well as the deformational and field effects in it.
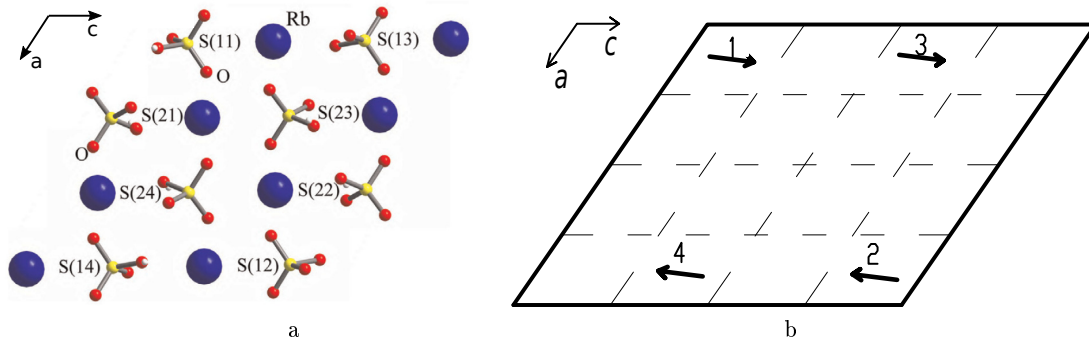

Fig. 1. The primitive cell of RbHSO$_4$ (a) and the scheme of the orientation of effective dipole moments $\mathbf{d}_{qf}$ of the sulphate groups $(SO_4)_{1f}$ in the paraelectric phase (b)

In the present paper, we use the model of [1] to explore the behavior of the dynamic dielectric permittivity of RbHSO$_4$ at different values of hydrostatic pressure.

II. FOUR-SUBLATTICE MODEL OF A DEFORMED CRYSTAL

In order to calculate the thermodynamic characteristics of RbHSO$_4$, we use the model [1] and take into account the presence of four structural units (sulphate complexes $(SO_4)_{11}$, $(SO_4)_{12}$, $(SO_4)_{13}$, $(SO_4)_{14}$) in the

primitive cell, which move in double asymmetric potential wells. We ascribe to these units the dipole moments $\mathbf{d}_{qf}$, where q is the primitive cell index; f is the index of the dipole moment within the cell ($f = 1, \ldots, 4$). In the paraelectric phase, the sum of these moments is equal to zero; their orientations are shown in Fig. 1,b. The changes $\Delta\mathbf{d}_{qf}$ are responsible for the appearance of spontaneous polarization in the ferroelectric phase.

The pseudospin variables $\frac{\sigma_{q1}}{2}, \ldots, \frac{\sigma_{q4}}{2}$ describe the reordering of the dipole moments associated with the structure elements $\mathbf{d}_{qf} = \boldsymbol{\mu}_f \frac{\sigma_{qf}}{2}$. The mean values of $\langle \frac{\sigma}{2} \rangle = \frac{1}{2}(n_a - n_b)$ are connected to the differences in the

populations of the two possible equibrium positions of groups $(SO_4)_{1f}$: n_a and n_b.

The model Hamiltonian in the pseudospin representation reads:

$$\hat{H} = NU_{\text{seed}} - \frac{1}{2} \sum_{qq'} \sum_{f,f'=1}^{4} J_{ff'}(qq') \frac{\sigma_{qf}}{2} \frac{\sigma_{q'f'}}{2} \quad (1)$$

$$- \sum_{q} \sum_{f=1}^{4} (\Delta_f + \boldsymbol{\mu}_f \mathbf{E}) \frac{\sigma_{qf}}{2},$$

where N is the number of the primitive cells.

The term U_{seed} in (2) is the "seed" energy, which corresponds to the lattice of heavy ions and is not explicitly dependent on the configuration of the pseudospin subsystem. It includes the elastic, piezoelectric, and dielectric parts, expressed via the electric fields E_i ($i = 1, 2, 3$) and strains u_j ($j = 1, \ldots, 6$) [1]:

$$U_{\text{seed}} = v \Big(\frac{1}{2} \sum_{j,j'=1}^{6} c_{jj'}^{0}(T) u_j u_{j'} \quad (2)$$

$$- \sum_{i=1}^{3} \sum_{j=1}^{6} e_{ij}^{0} u_j E_i - \sum_{i,i'=1}^{3} \frac{1}{2} \chi_{ii'}^{u0} E_i E_{i'} \Big).$$

The parameters $c_{jj'}^{0}(T)$, e_{ij}^{0}, χ_{ij}^{u0} are the so-called seed elastic constants, piezoelectric stress coefficients, and dielectric susceptibilities; v is the primitive cell volume.

The second term in (2) describes the interactions between the pseudospins, taken into account in the mean field approximation

$$- \frac{1}{2} \sum_{qq'} \sum_{f,f'=1}^{4} J_{ff'}(qq') \frac{\sigma_{qf}}{2} \frac{\sigma_{q'f'}}{2} \quad (3)$$

$$= \frac{1}{2} \sum_{\substack{qq' \\ ff'}} J_{ff'}(qq') \frac{\eta_f}{2} \frac{\eta_{f'}}{2} - \sum_{\substack{qq' \\ ff'}} J_{ff'}(qq') \frac{\eta_{f'}}{2} \frac{\sigma_{qf}}{2}.$$

Here σ_{qf} is the z-component of the operator of the pseudospin, situated in the q-th cell at the sulphate group $(SO_4)_{1f}$ ($f = 1, 2, 3, 4$), $\eta_f = \langle \sigma_{qf} \rangle$.

The third term in (2) describes the interaction of the pseudospins with the external electric field $\mathbf{E}$ and with the local fields Δ_f. The $\boldsymbol{\mu}_f$ parameters are the effective dipole moments per one pseudospin $\boldsymbol{\mu}_1 = \boldsymbol{\mu}_2 = (\mu^x, \mu^y, \mu^z)$, $\boldsymbol{\mu}_3 = \boldsymbol{\mu}_4 = (\mu^x, -\mu^y, \mu^z)$.

The Fourier-transforms of the interaction constants $J_{ff'} = \sum_{q'} J_{ff'}(qq')$ at $\mathbf{k} = 0$ and the local fields Δ_f are linearly expanded over the strains u_j:

$$J_{ff'} = J_{ff'}^{0} + \sum_{j} \psi_{ff'j} u_j, \quad \Delta_f = \Delta_f^{0} + \sum_{j} \varphi_{fj} u_j. \ (4)$$

Taking into account the crystal symmetry, the parameters $J_{ff'}$ read

$$J_{\frac{11}{22}} = J_{11}^{0} + \sum_{l=1,2,3,5} \psi_{11l} u_l + \psi_{114} u_4 + \psi_{116} u_6,$$

$$J_{\frac{33}{44}} = J_{11}^{0} + \sum_{l} \psi_{11l} u_l - \psi_{114} u_4 - \psi_{116} u_6, \quad (5)$$

$$J_{\frac{12}{34}} = J_{12}^{0} + \sum_{l} \psi_{12l} u_l \pm \psi_{124} u_4 \pm \psi_{126} u_6,$$

$$J_{\frac{13}{24}} = J_{13}^{0} + \sum_{l} \psi_{13l} u_l, \quad J_{\frac{14}{23}} = J_{14}^{0} + \sum_{l} \psi_{14l} u_l,$$

$$\Delta_{\frac{1}{3}} = \Delta_1^{0} + \sum_{l} \varphi_{1l} u_l \pm \varphi_{14} u_4 \pm \varphi_{16} u_6,$$

$$\Delta_{\frac{2}{4}} = -\Delta_1^{0} - \sum_{l} \varphi_{1l} u_l \mp \varphi_{14} u_4 \mp \varphi_{16} u_6.$$

As a result, in the mean field approximation the initial Hamiltonian (2) reads:

$$\hat{H} = NU_{\text{seed}} + \frac{N}{8} \sum_{ff'} J_{ff'} \eta_f \eta_{f'} - \sum_{q} \sum_{f=1}^{4} \mathcal{H}_f \frac{\sigma_{qf}}{2}, (6)$$

where

$$\mathcal{H}_f = \frac{1}{2} \sum_{f'} J_{ff'} \eta_{f'} + \Delta_f + \boldsymbol{\mu}_f \mathbf{E}. \quad (7)$$

In [1], the system of equations for the order parameters η_f and strains u_j

$$\eta_f = \tanh \frac{\beta}{2} \mathcal{H}_f. \quad (8)$$

$$\sigma_j = \sum_{j'=1}^{6} c_{jj'}^{0}(T) u_{j'} - \sum_{i=1}^{3} e_{ij}^{0} E_i \quad (9)$$

$$- \sum_{f,f'=1}^{4} \frac{\psi_{ff'j}}{8v} \eta_f \eta_{f'} - \sum_{f=1}^{4} \frac{\varphi_{fj}}{2v} \eta_f,$$

and the polarization vector components

$$P_i = \sum_{j=1}^{6} e_{ij}^{0} u_j + \sum_{i'=1}^{3} \chi_{ii'}^{u0} E_{i'} + \frac{1}{2v} \sum_{f=1}^{4} \mu_f^{(i)} \eta_f, \quad (10)$$

have been obtained.

III. DYNAMIC DIELECTRIC PROPERTIES OF A CLAMPED RbHSO₄ CRYSTAL. ANALYTICAL RESULTS

Hereafter we study the longitudinal dynamic dielectric characteristics, when the shear stresses are absent. In this case the shear strains u_4 and u_6 are equal to zero. We use the approach based on the ideas of the Glauber stochastic model. In this approach the following system of the Glauber equations for the time-dependent one-particle correlation functions of pseudospins is obtained

$$- \alpha \frac{d}{dt} \langle \sigma_{qf} \rangle = \langle \sigma_{qf} [1 - \sigma_{qf} \tanh \frac{1}{2} \beta \varepsilon_{qf}(t)] \rangle, \quad (11)$$

where the α parameter sets the time scale of the dynamic processes in the sytem; $\varepsilon_{qf'}(t)$ is the local field acting on the f'th pseudospin in the qth cell; this is the factor at $\sigma_{qf'}/2$ in the initial Hamiltonian. In the mean field approximation, the local fields $\varepsilon_{qf}(t)$ are the factors at $\sigma_{qf}/2$ in the one-particle Hamiltonians (7):

$$\varepsilon_{qf} = \mathcal{H}_f = \frac{1}{2}\sum_{f'} J_{ff'}\eta_{f'} + \Delta_f + \mu_f^z E_z. \qquad (12)$$

As a result, from (11) we obtain the following system of equations for the mean values of pseudospins $\langle\sigma_{qf}\rangle = \eta_f$

$$\alpha\frac{d}{dt}\eta_f = -\eta_f + \tanh\frac{\beta\mathcal{H}_f}{2}. \qquad (13)$$

In the solution of Eqs. (13) we shall restrict our consideration to the case of small deviations from equilibrium. To this end, we present η_f and the effective fields $\mathcal{H}_f$ as sums of the equilibrium parts of the quantities and their fluctuation parts (mechanically clamped crystal), and also expand $\tanh(\ldots)$ in series over $\mathcal{H}_f$, retaining only the zeroth order and linear terms

$$\eta_f = \tilde{\eta}_f + \eta_{ft}, \qquad (14)$$

$$\mathcal{H}_f = \tilde{\mathcal{H}}_f + \mathcal{H}_{ft}$$
$$= \frac{1}{2}\sum_{f'} J_{ff'}\tilde{\eta}_{f'} + \Delta_f + \mu_f^z E_z + \frac{1}{2}\sum_{f'} J_{ff'}\eta_{f't} + \mu_f^z E_{zt}.$$

$$\tanh\frac{\beta\mathcal{H}_f}{2} = \tanh\frac{\beta\tilde{\mathcal{H}}_f}{2} + K_f\frac{\beta\mathcal{H}_{ft}}{2},$$

$$K_f = 1 - (\tanh\frac{\beta\tilde{\mathcal{H}}_f}{2})^2 = 1 - \tilde{\eta}_f^2.$$

Substituting (14) into (13) and taking into account Eq.(8), obeyed at equilibrium, we obtain the system of equations for the non-equilibrium contributions to the order parameters

$$\alpha\frac{d}{dt}\eta_{ft} = -\eta_{ft} + K_f\frac{\beta}{2}\left(\frac{1}{2}\sum_{f'} J_{ff'}\eta_{f't} + \mu_f^z E_{zt}\right). \ (15)$$

In the presence of the field E_{zt}, from the symmetry considerations it follows that $\eta_{1t} = \eta_{3t}$, $\eta_{2t} = \eta_{4t}$, $\mu_f^z = \mu^z$, and the system of equations (15) reads:

$$\alpha\frac{d}{dt}\eta_{1t} = -\eta_{1t} + K_1\frac{\beta}{2}\left[\frac{1}{2}(J_{11} + J_{13})\eta_{1t}\right.$$
$$\left. + \frac{1}{2}(J_{12} + J_{14})\eta_{2t} + \mu^z E_{zt}\right], \qquad (16)$$

$$\alpha\frac{d}{dt}\eta_{2t} = -\eta_{2t} + K_2\frac{\beta}{2}\left[\frac{1}{2}(J_{21} + J_{23})\eta_{1t}\right.$$
$$\left. + \frac{1}{2}(J_{22} + J_{24})\eta_{2t} + \mu^z E_{zt}\right].$$

We can rewrite the system (16) in a more convenient form:

$$\frac{d}{dt}\begin{pmatrix}\eta_{1t}\\\eta_{2t}\end{pmatrix} = \begin{pmatrix}a_{11} & a_{12}\\a_{21} & a_{22}\end{pmatrix}\begin{pmatrix}\eta_{1t}\\\eta_{2t}\end{pmatrix} + \begin{pmatrix}b_1\\b_2\end{pmatrix}\beta\mu^z E_{zt}, (17)$$

where

$$a_{11} = \left(-1 + K_1\frac{\beta}{4}(J_{11} + J_{13})\right)/\alpha,$$

$$a_{12} = K_1\frac{\beta}{4\alpha}(J_{12} + J_{14}), \quad b_1 = \frac{K_1}{2\alpha}$$

$$a_{21} = K_2\frac{\beta}{4\alpha}(J_{21} + J_{23}),$$

$$a_{22} = \left(-1 + K_2\frac{\beta}{4}(J_{22} + J_{24})\right)/\alpha, \quad b_2 = \frac{K_2}{2\alpha}. \ (18)$$

Solving Eqs. (17), we obtain the time-dependent mean values of the pseudospins. Substituting the solutions of (17) into (10) and differentiating the results with respect to the field, we obtain the expression for the dynamic dielectric susceptibility.

$$\chi_{33}(\omega) = \chi_{33}^0 + \lim_{E_{3t}\to 0}\frac{\mu^z}{v}\frac{d(\eta_{1t} + \eta_{3t})_3}{dE_{3t}},$$

The obtained components of the susceptibility consist of the "seed" contribution and two relaxational modes

$$\chi_{33}(\omega) = \chi_{33}^0 + \sum_{l=1}^{2}\frac{\chi_l}{1 + i\omega\tau_l}, \qquad (19)$$

where

$$\chi_l = \frac{\beta}{v}\frac{\tau_1\tau_2(\mu^z)^2}{\tau_2 - \tau_1}(-1)^{l-1}\left\{b_1 + b_2\right.$$
$$\left. + \tau_l[b_1 a_{22} + b_2 a_{11} - (b_1 a_{21} + b_2 a_{12})]\right\},$$

$\tau_{1,2}$ are the relaxation times

$$(\tau_{1,2})^{-1} = \frac{1}{2}\left\{-(a_{11} + a_{22})\right.$$
$$\left. \pm\sqrt{(a_{11} + a_{22})^2 - 4(a_{11}a_{22} - a_{12}a_{21})}\right\}. \qquad (20)$$

The components of the dynamic dielectric permittivity of the pseudospin subsystem of GPI read

$$\varepsilon_{33}(\omega) = 1 + 4\pi\chi_{33}(\omega). \qquad (21)$$

IV. COMPARISON OF THE NUMERICAL CALCULATIONS WITH EXPERIMENTAL DATA

The values of the model parameters have been determined in [1] by fitting the calculated characteristics to experimental data for the temperature dependences of the spontaneous polarization $P_3(T)$ [3, 10], dielectric permittivity $\varepsilon_{33}(T)$ in the absence of external influence [3, 10, 11] and at different values of hydrostatic pressure [2] and electric field [12], molar specific heat $C(T)$ [13], and elastic constants $c_{jj'}(T)$ [11].

The interaction constants in an undeformed crystal $J_{ff'}^0$ $(f, f' = 1, 2, 3, 4)$ and the local fields Δ_f^0, creating the asymmetry in the populations of the two equilibrium positions are as follows $J_{11}^0/k_B = J_{13}^0/k_B = 372$ K, $J_{12}^0/k_B = J_{14}^0/k_B = 310$ K, $\Delta_1^0/k_B = 244.81$ K. The rest

of the parameters $J^0_{ff'}$ and Δ^0_f are determined by the crystal symmetry of RbHSO$_4$, as discussed in (5).

The deformation potentials $\psi_{ff'j}$ and φ_{fj} are: $\tilde{\psi}_{111} = -1700$ K, $\tilde{\psi}_{112} = -4600$ K, $\tilde{\psi}_{113} = -500$ K, $\tilde{\psi}_{114} = 0$ K, $\tilde{\psi}_{115} = 1200$ K, $\tilde{\psi}_{116} = 3500$ K, $\tilde{\psi}_{121} = -500$ K, $\tilde{\psi}_{122} = -3040$ K, $\tilde{\psi}_{123} = -500$ K, $\tilde{\psi}_{124} = 0$ K, $\tilde{\psi}_{125} = 400$ K, $\tilde{\psi}_{126}/k_\mathrm{B} = -7000$ K, $\tilde{\psi}_{ff'j} = \psi_{ff'j}/k_\mathrm{B}$. The analysis shows that the calculated thermodynamic characteristics depend on the sums $\psi_{11l}+\psi_{13l}$, $\psi_{12l}+\psi_{14l}$ ($l = 1, 2, 3, 5$). For simplicity's sake, we take them to be equal, $\psi_{13l} = \psi_{11l}$, $\psi_{14l} = \psi_{12l}$. The rest of the parameters $\psi_{ff'j}$ are determined by the crystal symmetry of RbHSO$_4$, as discussed in (5), $\varphi_{fj} = 0$ K.
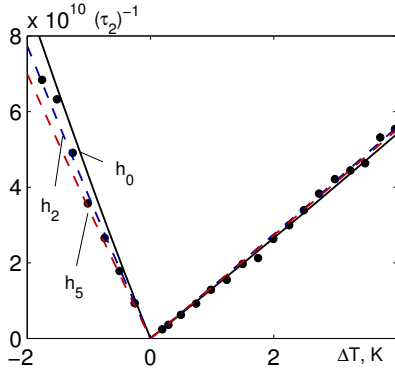

Fig. 2. The temperature dependence of the inverse relaxation time $(\tau_2)^{-1}$ at different values of hydrostatic pressure. The lower index in h_p denotes the value of pressure p (kbar). The solid circles ($\bullet$) correspond to the data from [14]
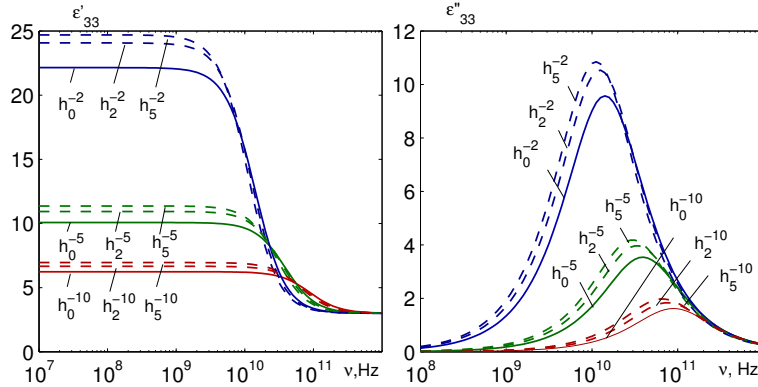
The effective dipole moment equals $\mu^z = 2.8 \cdot 10^{-30}$ C·m.

The "seed" dielectric susceptibility $\chi^{u0}_{ii'}$, piezoelectric stress coefficients e^0_{ij}, and elastic constants c^0_{ij} are: $\chi^{u0}_{33} = 0.159$ (note that in [1] we took it to be equal to 0.35), $\chi^{u0}_{13} = 0.0$; $e^0_{ij} = 0 \frac{\mathrm{C}}{\mathrm{m}^2}$;

$c^0_{11} = 3.06 \cdot 10^{10} \frac{\mathrm{N}}{\mathrm{m}^2}$, $\quad c^0_{12} = 1.54 \cdot 10^{10} \frac{\mathrm{N}}{\mathrm{m}^2}$, $c^0_{13} = 0.8 \cdot 10^{10} \frac{\mathrm{N}}{\mathrm{m}^2}$,

$c^0_{22} = 3.8 \cdot 10^{10} \frac{\mathrm{N}}{\mathrm{m}^2}$, $\quad c^0_{23} = 0.67 \cdot 10^{10} \frac{\mathrm{N}}{\mathrm{m}^2}$, $c^0_{33} = 3.62 \cdot 10^{10} \frac{\mathrm{N}}{\mathrm{m}^2}$,

$c^0_{44} = 0.48 \cdot 10^{10} \frac{\mathrm{N}}{\mathrm{m}^2}$, $\quad c^0_{55} = 0.53 \cdot 10^{10} \frac{\mathrm{N}}{\mathrm{m}^2}$, $c^0_{66} = 1.25 \cdot 10^{10} \frac{\mathrm{N}}{\mathrm{m}^2}$,

$c^0_{15} = c^0_{25} = c^0_{35} = c^0_{46} = 0.0 \frac{\mathrm{N}}{\mathrm{m}^2}$.

The primitive cell volume of RHS is $v = 0.842 \cdot 10^{-27}$ m^3.

The parameter $\alpha = P + R|T - T_c|$, where $P = 1.6 \cdot 10^{-14}$ s, $R = -0.011 \cdot 10^{-14}$ s.

There are two contributions to the components of the dynamic dielectric permittivity tensor in the RbHSO$_4$ crystal. Only one of these contributions to the permittivities is crucial ($\chi_2 \gg \chi_1$); the respective relaxation times are $\tau_2 \gg \tau_1$. Related to the relaxation time τ_2^y is the typical of this crystal relaxation frequency $\nu_s = (2\pi\tau_2)^{-1}$, which nominally separates the regions of the low-frequency and high-frequency dynamics of the system.

Fig. 3. The frequency dependences of the real ε'_{33} and imaginary ε''_{33} parts of the dielectric permittivity of RbHSO$_4$ at different values of ΔT and hydrostatic pressure p (kbar). In the quantity $h^{\Delta T}_p$ the upper index denotes the temperature $\Delta T = -2.0$ K; $\Delta T = -5.0$ K; $\Delta T = -10.0$ K, whereas the lower index denotes the pressure magnitude

Influence of hydrostatic pressure on the relaxation time is illustrated in Fig. 2 by plotting the temperature curves of $(\tau_2)^{-1}$ at different values of pressures.

The magnitude of $(\tau_1)^{-1}$ decreases as the system approaches the transition temperature and tends to zero at $T = T_c$. As one can see in Fig. 2, hydrostatic pressure decreases $(\tau_1)^{-1}$ at the fixed ΔT in the ferroelectric phase, and first slightly increases and then (at high pressures) decreases $(\tau_1)^{-1}$ in the paraelectric phase.

As a result, the dispersion region in the frequency dependences of $\varepsilon'_{33}(\nu)$ and $\varepsilon''_{33}(\nu)$ shifts to lower frequencies in the presence of pressure in the ferroelectric phase (dashed lines in Fig. 3), as compared to the solid lines, corresponding to the ambient pressure. In the paraelectric phase, the dispersion region at low pressures (dashed lines in Fig. 4) shifts to higher frequencies, as compared to the solid lines for the ambient pressure, and then shifts back to lower frequencies at higher pressures.

Below the dispersion and in the ferroelectric phase, the curves $\varepsilon'_{33}(p, \nu)$ and $\varepsilon''_{33}(p, \nu)$ in the presence of pressure p_h run higher than the corresponding curves at ambient pressure (Fig. 3); the opposite is observed in the

paraelectric phase (Fig. 4). This is due to the increase in the static permittivity by hydrostatic pressure in the ferroelectric phase and to the decrease in the paraelectric phase.

In Figs. 5, 6, and 7, we plot the temperature dependences of the real ε'_{33} and imaginary ε''_{33} parts of the dielectric permittivity of RbHSO$_4$ at different frequencies ν (low frequencies: Fig. 5, intermediate frequencies: Fig. 6, high frequencies: Fig. 7) and different values of pressure p_h.
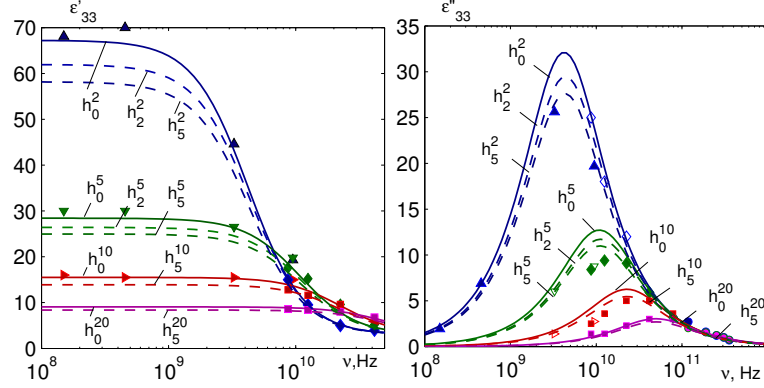

Fig. 4. The frequency dependences of the real ε'_{33} and imaginary ε''_{33} parts of the dielectric permittivity of RbHSO$_4$ at different ΔT and different values of hydrostatic pressure p (kbar). In the quantity $h_p^{\Delta T}$ the upper index denotes $\Delta T = 2.0$ K — ▲ [14], ♦ [15], ● [16]; $\Delta T = 5.0$ K — ▼ [14], ♦ [15]; $\Delta T = 10.0$ K — ► [14], ■ [15]; $\Delta T = 20$ K — ■ [15], ● [16], and the lower index denotes the pressure magnitude (kbar)
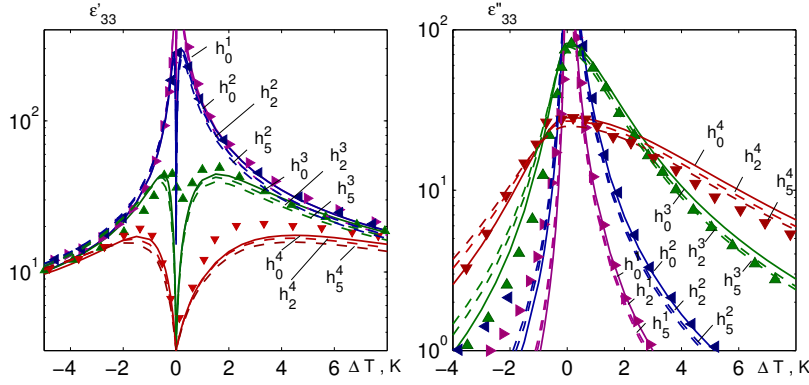
Fig. 5. The temperature dependences of the real ε'_{33} and imaginary ε''_{33} parts of the dielectric permittivity of RbHSO$_4$ at different frequencies ν (GHz) and different values of pressure p_h. In the quantity h_p^i the upper index denotes the frequency (GHz) $0.105 - 1$, ► [14]; $0.455 - 2$, ◄ [14]; $3.27 - 3$, ▲ [14]; $9.50 - 4$, ▼ [14], and the lower index denotes the pressure magnitude (kbar)
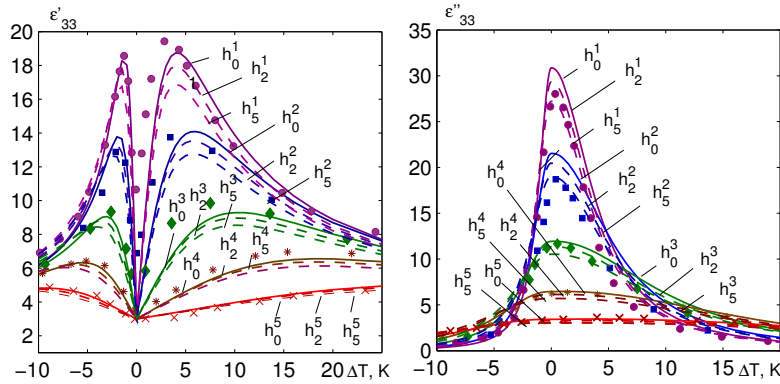
Fig. 6. The temperature dependences of the real ε'_{33} and imaginary ε''_{33} parts of the dielectric permittivity of RbHSO$_4$ at different frequencies ν (GHz) and different values of pressure p_h. In the quantity h_p^i the upper index denotes the frequency (GHz) $8.72 - 1$, ● [17]; $12.5 - 2$, ■ [17]; $22.55 - 3,3'$, ♦ [17]; $41.7 - 4$, * [17]; $78.5 - 3$, × [17], and the lower index denotes the pressure magnitude (kbar)
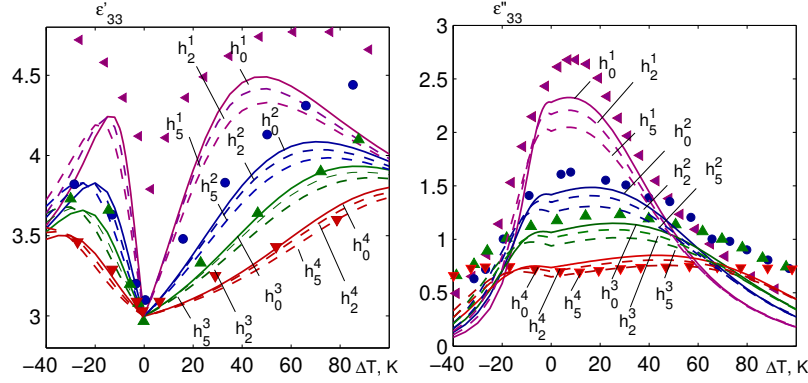
Fig. 7. The temperature dependences of the real ε'_{33} and imaginary ε''_{33} parts of the dielectric permittivity of RbHSO$_4$ at different frequencies ν (GHz) and different values of pressure p_h. In the quantity h^i_p the upper index denotes the frequency (GHz) $118 - 1$, ◄ [16]; $190 - 2$, ● [16]; $253 - 3$, ▲ [16]; $366 - 4$, ▼ [16], and the lower index denotes the pressure magnitude (kbar)

As one can see, in the ferroelectric phase at temperatures far from T_c, the magnitude of the dielectric permittivity ε'_{33} in the presence of the pressure (dashed lines) is larger than at ambient pressure (solid lines), which is due to the above mentioned increase in the static permittivity with pressure. At temperatures close to T_c, the values of ε'_{33} are lower than at ambient pressure due to the increase in the relaxation time with pressure. In the paraelectric phase, the permittivity ε'_{33} in the presence of pressure is smaller than at ambient pressure at all temperatures, both close and far from T_c. This is due to the decrease of the static permittivity with pressure and a weak influence of the pressure on the relaxation time in the paraelectric phase.

V. CONCLUSIONS

The model of deformed RbHSO$_4$ predicts a linearly increasing dependence of the Curie temperature on hydrostatic pressure. The phase transition remains of the first order. In the ferroelectric phase, the hydrostatic pressure increases the relaxation time and shifts the dispersion region to lower frequencies. The magnitude of the dielectric permittivity increases. In the paraelectric phase, the relaxation time first slightly decreases with pressure, and then slightly increases. As a result, the dispersion region at low pressures shifts to higher frequencies, but as the pressure increases, shifts back to lower frequencies. The magnitude of the dielectric permittivity decreases with pressure.

[1] A. S. Vdovych, R. R. Levitskii, I. R. Zachek. J. Phys. Stud. **24**, 2702 (2020); https://doi.org/10.30970/jps.24.2702.

[2] K. Gesi, K. Ozawa, J. Phys. Soc. Jpn. **38**, 459 (1975); https://doi.org/10.1143/JPSJ.38.459.

[3] R. Pepinsky, K. Vedam, Phys. Rev. **117**, 1502 (1960); https://doi.org/10.1103/PhysRev.117.1502.

[4] J. P. Ashmore, H. E. Petch, Can. J. Phys. **53**, 2694 (1975); https://doi.org/10.1139/p75-328.

[5] K. Iton, H. Ohno, S. Kuragaki, J. Phys. Soc. Jpn. **64**, 479 (1995); https://doi.org/10.1143/JPSJ.64.479.

[6] I. R. Zachek, Ya. Shchur, R. R. Levitskii, Physica B **478**, 113 (2015); https://doi.org/10.1016/j.physb.2015.08.058.

[7] I. R. Zachek, R. R. Levitskii, Ya. Shchur, O. B. Bilenka, Condens. Matter Phys. **18**, 43703 (2015); https://doi.org/10.5488/CMP.18.43703.

[8] I. R. Zachek, R. R. Levitskii, A. S. Vdovych, J. Phys. Stud. **19**, 3703 (2015); https://doi.org/10.30970/jps.19.3703.

[9] I. R. Zachek, R. R. Levitskii, A. S. Vdovych, M. C. Karkuljevska, Phys. Chem. Solid State **16**, 276 (2015); https://doi.org/10.15330/pcss.16.2.276-283.

[10] H. Kajikawa, T. Ozaki, E. Nakamura, J. Phys. Soc. Jpn. **43**, 937 (1977); https://doi.org/10.1143/JPSJ.43.937.

[11] M. P. Zajceva, L. A. Shabanova, L. I. Zherebcova, Fiz. Tverd. Tela **21**, 2308 (1979).

[12] E. Nakamura, H. Kajikawa J. Phys. Soc. Jpn. **44**, 519 (1978); https://doi.org/10.1143/JPSJ.44.519.

[13] K. S. Alexandrov *et al.*, Ferroelectrics **12**, 191 (1976); https://doi.org/10.1080/00150197608241423.

[14] T. Ozaki. J. Phys. Soc. Jpn. **49**, 234 (1980); https://doi.org/10.1143/JPSJ.49.234.

[15] J. Grigas *et al.*, Liet. Fiz. Rink. **24**, 33 (1984).

[16] V. S. Ambrazjavichene, A. A. Volkov , G. V. Kozlov, V. S. Krasikov, E. B. Krjukova, Phys. Tver. Tela **25**, 1605 (1983).

[17] W. Paprotny, J. Grigas, R. R. Levitsky, I. V. Kutny, V. S. Krasikov, Ferroelectrics **61**, 19 (1984); https://doi.org/10.1080/00150198408018932.

ВПЛИВ ГІДРОСТАТИЧНОГО ТИСКУ НА ДИНАМІЧНІ ДІЕЛЕКТРИЧНІ ХАРАКТЕРИСТИКИ RbHSO$_4$

А. С. Вдович[1], Р. Р. Левицький[1], І. Р. Зачек[2], А. П. Моїна[1]

[1]*Інститут фізики конденсованих систем НАН України,*
вул. Свенціцького, 1, Львів, 79011, Україна,

[2]*Національний університет "Львівська політехніка",*
вул. С. Бандери, 12, 79013, Львів, Україна

Сеґнетоелектрик із водневими зв'язками RbHSO$_4$ є прикладом кристала, де перехід із високотемпературної парафази в низькотемпературну сеґнетофазу пов'язаний з упорядкуванням не протонів, а сульфатних груп SO$_4$, які стрибають між двома положеннями рівноваги. На основі модифікованої чотирипідґраткової псевдоспінової моделі деформованого сеґнетоелектрика RbHSO$_4$ у межах методу Ґлаубера в наближенні молекулярного поля отримано систему рівнянь для часозалежних середніх значень псевдоспінів. Цю систему рівнянь розв'язано для малих відхилень від рівноваги як відгук на мале зовнішнє часозалежне поле. Також знайдено вираз для часів релаксації.

Упохіднивши динамічний розв'язок за полем, отримали вираз для поздовжньої динамічної діелектричної проникності механічно затиснутого кристала. Одержана динамічна діелектрична проникність складається з двох внесків із відповідними часами релаксації. Один із цих внесків і відповідний йому час релаксації на три порядки більший за інший. Тобто діелектрична проникність має практично монодисперсний характер. За малих частот діелектрична проникність поводиться як статична; за частот, сумірних з оберненим часом релаксації, спостерігається релаксаційна дисперсія; за великих частот проявляється лише ґратковий внесок у діелектричну проникність, а псевдоспіновий практично зникає. Досліджено вплив гідростатичного тиску на динамічну діелектричну проникність у широкому температурному й частотному діапазонах.

Установлено, що гідростатичний тиск у сеґнетофазі збільшує час релаксації та зсуває ділянку дисперсії діелектричної проникності в бік нижчих частот. Водночас діелектрична проникність зростає за величиною. У парафазі час релаксації за наявності тиску спочатку слабо зменшується, а за великих тисків знову слабо зростає. У результаті ділянка дисперсії за малих тисків дещо зсувається до вищих частот, а з подальшим збільшенням тиску знову зсувається до нижчих частот. Водночас діелектрична проникність зменшується за величиною під дією тиску. Отримано задовільний кількісний опис відповідних експериментальних даних.

Ключові слова: сеґнетоелектрики, діелектрична проникність, ефекти тиску.